

Stability of the spin-1/2 kagome ground state with breathing anisotropy

Cécile Repellin¹, Yin-Chen He², and Frank Pollmann³

¹ *Max-Planck-Institut für Physik komplexer Systeme, 01187 Dresden, Germany*

² *Department of Physics, Harvard University, Cambridge, Massachusetts, 02138, USA*

³ *Technische Universität München, Physics Department T42, 85747 Garching, Germany*

(Dated: July 3, 2017)

We numerically study the spin-1/2 breathing kagome lattice. In this variation of the kagome Heisenberg antiferromagnet, the spins belonging to upward and downward facing triangles have different coupling strengths. Using the density matrix renormalization group (DMRG) method and exact diagonalization, we show that the kagome antiferromagnet spin liquid is extremely robust to this anisotropy. Materials featuring this anisotropy – and especially the recently studied vanadium compound $[\text{NH}_4]_2[\text{C}_7\text{H}_{14}\text{N}][\text{V}_7\text{O}_6\text{F}_{18}]$ (DQVOF) – may thus be very good candidates to realize the much studied kagome spin liquid. Further, we closely examine the limit of strong breathing anisotropy and find indications of a transition to a nematic phase.

I. INTRODUCTION

Quantum spin liquids¹ (QSLs) are strongly correlated phases which cannot be characterized by a spontaneous symmetry breaking at zero temperature. These highly entangled states feature exotic fractionalized spin excitations^{2,3}, and have thus received a lot of theoretical and experimental interest^{1,4-6}. Frustrated magnets, where the strong quantum fluctuations prevent the magnetic ordering of the spins, are a fertile ground to realize such states. While there is substantial evidence that various candidate materials might present spin liquid-like behavior, the absence of a local order parameter makes it very hard to identify QSLs experimentally. To overcome these difficulties, a theoretical understanding of the underlying models is essential.

The spin $S = 1/2$ kagome lattice with nearest-neighbor Heisenberg interactions (KAFM) is one of the prime candidates to realize a QSL. Despite intense research during the last few decades⁷⁻¹⁹, the KAFM is still not fully understood. While there is a consensus that the ground state is a QSL, it is still not fully agreed upon whether it is gapped or gapless. A gapped \mathbb{Z}_2 spin liquid^{18,19} is supported by early DMRG results, but a recent DMRG study brought a new perspective on the problem by unveiling signatures of Dirac cones in the transfer matrix spectrum of the ground state²⁰. These signatures are compatible with earlier variational calculations showing a competitive energy for a gapless $U(1)$ Dirac spin liquid¹⁶. On the experimental side, there is a growing number of candidate materials, such as herbertsmithite²¹, volborithite^{22,23} or vesignieite²⁴. Various perturbations modify the KAFM in these materials, such as impurities, as well as spatial or spin anisotropy or Dzyaloshinskii-Moriya interactions.

Recently, a vanadium-based compound – $[\text{NH}_4]_2[\text{C}_7\text{H}_{14}\text{N}][\text{V}_7\text{O}_6\text{F}_{18}]$ or diammonium quinclidinium vanadium(III,IV) oxyfluoride (DQVOF) – has received significant attention. Experiments^{25,26} have shown the absence of magnetic ordering at low temperature, as well as signatures of a gapless spin liquid^{26,27}. In this material, the d^1 ions V^{4+} – instead of the more usual

d^9 Cu^{2+} – form an array of kagome layers separated by V^{3+} triangular interlayers. This offers alternative properties which make DQVOF a promising kagome QSL candidate. The use of V^{4+} indeed avoids the intrinsic stoichiometric defects due to the substitution of Zn^{2+} ions in herbertsmithite, and Ref. 25 reported the absence of any V^{3+} defects. Thanks to relatively small interactions between the kagome and intermediary layers^{25,26}, the two-dimensional approximation is also better verified than in herbertsmithite. Moreover, this V^{4+} material may circumvent the important Jahn-Teller distortions that lower the symmetry of Cu^{2+} -based kagome systems²⁵. While equilateral, the triangles of the kagome lattice of DQVOF differ in size, resulting in an anisotropy of the exchange coupling between spins belonging to the upward and downward facing triangles, or breathing anisotropy. This raises an important question: are the signatures observed in DQVOF a result of the breathing anisotropy, or are they generic features of a kagome spin liquid?

Beyond the modeling of realistic materials, the numerical study of the breathing kagome model is also motivated by more theoretical aspects. Recently, various microscopic terms have been considered to drive the KAFM to one of its neighboring phases. For example, sufficiently strong longer range interactions cause the system to spontaneously break time-reversal invariance and form a chiral spin liquid^{28,29}. Easy-plane and easy-axis anisotropy have also been shown to adiabatically connect the KAFM to the corresponding strong anisotropic limits³⁰⁻³². These approaches have brought important insights into the KAFM problem in recent years³³. We study the phase diagram of the breathing kagome model in a similar spirit. This deviation from the ideal kagome model is particularly interesting since it does not change the degeneracy of the classical ground state. The very anisotropic limit of this model has been considered in previous works³⁴⁻⁴⁰ as a strong coupling approach to the isotropic kagome model. However, the nature of the ground state in the strong breathing anisotropy limit remains unknown.

In this paper, we study the phase diagram of the

kagome model with breathing anisotropy. Using DMRG on infinitely long cylinders and exact diagonalization of finite toroidal clusters, we numerically show that the much studied kagome spin liquid is stable in a regime extending far beyond the value of the anisotropy measured in DQVOF. The robustness of the kagome spin liquid is supported by several numerical signatures, including low-energy spectra, entanglement entropy, correlation length and persisting signatures of Dirac cones in the transfer matrix spectrum. We also explore the very strongly anisotropic regime. Our finite-size results indicate a phase transition in this regime, leading to a nematic phase that preserves the translation but breaks the discrete lattice rotational symmetry of the system. We show that this state is adiabatically connected to the ground state of the first-order perturbation theory of the trimerized model³⁴. We also discuss the finite-size extrapolation of these results.

The remainder of the paper is organized as follows. In Sec. II, we give the details of the model and review the known physics of the strongly anisotropic limit. In Sec. III, we show the large robustness of the kagome spin liquid with breathing anisotropy by confronting the results of iDMRG and exact diagonalization. In Sec. IV, we focus on the strongly anisotropic limit. We identify a nematic state and discuss its stability in the thermodynamic limit.

II. DESCRIPTION OF THE MODEL AND LIMITING CASES

In this section, we present our model and review the isotropic and strongly anisotropic cases.

A. The kagome model

We study the spin-1/2 kagome lattice model with antiferromagnetic Heisenberg nearest-neighbor interactions and breathing anisotropy. The difference of size between the up and down triangles is accounted for by coupling constants of different strengths J_Δ and J_∇ (see Fig. 1). The Hamiltonian reads

$$H = J_\Delta \sum_{\langle i,j \rangle \in \Delta} \mathbf{S}_i \cdot \mathbf{S}_j + J_\nabla \sum_{\langle i,j \rangle \in \nabla} \mathbf{S}_i \cdot \mathbf{S}_j \quad (1)$$

where $\langle i,j \rangle$ represents neighboring sites belonging to the upward ($\langle i,j \rangle \in \Delta$) or downward ($\langle i,j \rangle \in \nabla$) facing triangles. Without loss of generality, we set $J_\nabla \leq J_\Delta$. The isotropic kagome lattice has the symmetry of the dihedral group D_6 . When $J_\nabla \neq J_\Delta$, inversion symmetry is broken, but rotations of order 3 and reflections are preserved, such that the symmetry group of the lattice is the dihedral group D_3 .

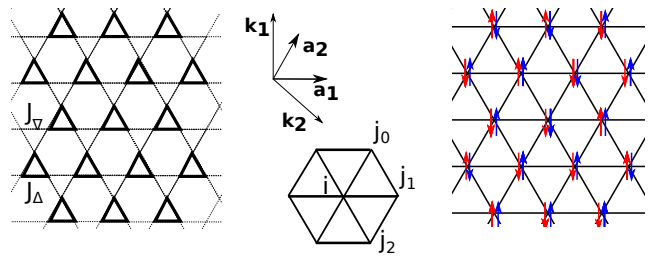


FIG. 1. Sketch of the breathing kagome lattice model. The *left panel* shows the exact model Eq. (1): neighboring spins belonging to an upward (resp. downward) facing triangle interact via a Heisenberg interaction of strength $J_\Delta = 1$ (resp. $J_\nabla < 1$). The weak and strong bonds of the Hamiltonian are represented with lines of different thickness. The Bravais lattice ($\mathbf{a}_1, \mathbf{a}_2$) and reciprocal lattice ($\mathbf{k}_1, \mathbf{k}_2$) vectors are also represented. The *right panel* sketches the kagome lattice in the strongly trimerized limit $J_\nabla/J_\Delta \ll 1$. In this limit, each set of three spins forming an upward triangle can be locally projected onto its $S = 1/2$ subspace leading to Eq. (5). This projection maps the kagome lattice model to an effective triangular lattice where each site has a pseudospin (red) and a spin (blue) degree of freedom. In the effective model, the interactions depend on the direction of the nearest-neighbor bond $\langle i, j_{0,1,2} \rangle$

B. The trimerized kagome model

Here, we focus on the limit $J_\nabla/J_\Delta \ll 1$ of the breathing kagome model Eq. (1), a limit known as the trimerized kagome model. Several variants^{34–38,41} of this limit have been considered in an effort to gain insight on the kagome antiferromagnet using a strong-coupling approach. We limit ourselves to the first-order perturbation theory in J_∇/J_Δ of the trimerized kagome model, which corresponds to a frustrated spin-orbital model on the triangular lattice.

Let us review this first-order strong-coupling expansion^{34–37}. One starts ($J_\nabla = 0$) with a lattice of uncoupled Δ triangles. A single triangle is described by the following Hamiltonian

$$\begin{aligned} h_\Delta &= \frac{J_\Delta}{2} \left[\left(\sum_{i=1}^3 \mathbf{S}_i \right)^2 - \sum_{i=1}^3 \mathbf{S}_i^2 \right] \\ &= \frac{J_\Delta}{2} \left[S^2 - \frac{9}{4} \right] \end{aligned} \quad (2)$$

where $S = \sum_{i=1}^3 \mathbf{S}_i$ is the total spin. The spectrum of one isolated triangle is thus made of two $S = 1/2$ doublets with energy $-3J_\Delta/4$, and one $S = 3/2$ quadruplet with energy $J_\Delta/4$. We note $|s_\pm\rangle$ the four $S = 1/2$ eigenstates of Eq. (2), where the upper index $s = \uparrow, \downarrow$ corresponds to the value of the magnetization $S_z = \pm 1/2$, while the lower index \pm is a pseudospin index. The state $|s_\pm\rangle$ may be chosen to be eigenstate of the chirality operator on a triangle. However, we find the following orthonormal basis choice^{35,38} to be more convenient since it does not

involve any complex numbers:

$$\begin{aligned} |s_+\rangle &= \frac{1}{\sqrt{2}} [|ss - s\rangle - |s - ss\rangle] \\ |s_-\rangle &= \frac{1}{\sqrt{6}} [|ss - s\rangle + |s - ss\rangle - 2|-sss\rangle] \end{aligned} \quad (3)$$

For a kagome lattice with N_s spins, the many-body basis $\{\Delta\}$ is obtained by considering all $4^{N_s/3}$ possible product states formed using the $|s_\pm\rangle$ single-triangle basis. The first-order perturbation theory thus yields:

$$H_{\text{eff}} = \mathcal{P}_{\{\Delta\}} H \mathcal{P}_{\{\Delta\}} \quad (4)$$

i.e. the projection of the original Hamiltonian Eq. (1) onto the basis $\{\Delta\}$. It yields an effective Hamiltonian H_{eff} on the triangular lattice with nearest-neighbor interactions entangling spin and pseudospin degrees of freedom. Note that the form of the interaction is determined by the direction of the link connecting the two neighbors. The effective Hamiltonian reads

$$\begin{aligned} H_{\text{eff}} &= -\frac{N_s}{4} \\ &+ J_{\nabla}/J_{\Delta} \sum_i \left[(\mathbf{S}_i \otimes I_i^C) \cdot (\mathbf{S}_{j_0} \otimes I_{j_0}^A) \right. \\ &\quad + (\mathbf{S}_i \otimes I_i^B) \cdot (\mathbf{S}_{j_1} \otimes I_{j_1}^A) \\ &\quad \left. + (\mathbf{S}_i \otimes I_i^B) \cdot (\mathbf{S}_{j_2} \otimes I_{j_2}^C) \right] \end{aligned} \quad (5)$$

where each value of i represents one site on the triangular lattice and \mathbf{S}_i is a spin-1/2 operator. j_0, j_1 and j_2 are three of the six nearest neighbors of site i whose position is specified in Fig. 1. I_i^A, I_i^B and I_i^C are operators acting on the pseudospin degree of freedom at site i . Their action can be represented by the following matrices

$$I^A = \begin{pmatrix} 1 & 0 \\ 0 & -1/3 \end{pmatrix} \quad (6)$$

$$I^B = \begin{pmatrix} 0 & 1/\sqrt{3} \\ 1/\sqrt{3} & 2/3 \end{pmatrix} \quad (7)$$

$$I^C = \begin{pmatrix} 0 & -1/\sqrt{3} \\ -1/\sqrt{3} & 2/3 \end{pmatrix} \quad (8)$$

The pseudospin degree of freedom may be seen as an orbital degree of freedom, such that H_{eff} describes a Kugel-Khomskii⁴² interaction on the triangular lattice. The entanglement of spin and orbital degrees of freedom in these models usually enhances the quantum fluctuations and can give rise to exotic phases of matter. On the triangular lattice, a large variety of phases has been predicted⁴³⁻⁴⁵ in spin-orbital models, including quantum spin liquids. Note, however, that these results were obtained after enforcing important symmetry constraints which do not apply to our model. While the spin degree of freedom is associated with an $SU(2)$ symmetry

inherited from the original spin model, the orbital degree of freedom in H_{eff} is not associated with an $SU(2)$ symmetry or any of its subgroups.

The nature of the ground state of the trimerized kagome model has been investigated in previous works in various ways. The nature of the ground state of H_{eff} was discussed in Ref. 35 based on a quantum dimer model whose large resonances were argued to lead to the formation of a spin liquid. To our knowledge, the only direct numerical study of H_{eff} was performed in the one-dimensional limit of a chain of coupled triangles³⁷. While most of our results are based on the numerical simulation of the full model Eq. (1), we will also use this effective trimerized model and relate its ground state to the ground state of the kagome model.

III. STABILITY OF THE KAGOME SPIN LIQUID UNDER BREATHING ANISOTROPY

In this section, we examine the properties of the ground state of the kagome model with breathing anisotropy described by Eq. (1). The DMRG algorithm has provided important insights into the nature of the ground state of the KAFM and some of its variants in the past and is thus a method of choice here. This method allows to efficiently obtain the ground state of our microscopic model on long cylinders. We also use exact diagonalization to obtain the low-energy spectrum in geometries preserving all the symmetries of the model. Finally, we extract the transfer matrix spectrum at various values of the breathing anisotropy, and show that the recent observation²⁰ of Dirac cone signatures in the isotropic model stays valid even for rather strong breathing anisotropy.

A. Properties of the ground state on an infinite cylinder: iDMRG results

We employ the infinite version of the DMRG algorithm⁴⁶⁻⁵⁰ (iDMRG) to compute the ground state of Eq. (1) on the cylinder geometry. The cylinder axis is along the x -direction, and the y axis coincides with one of the lattice axes. This geometry is commonly called YC2n, where $2n$ is the number of sites along the circumference. Cylinders which connect periodically across the cylinder with an additional two site shift along the x direction are denoted YC2n - 2. DMRG is a one-dimensional method that can also be used to find the ground state of two-dimensional systems by considering a chain forming a "snake" around the cylinder circumference. A translationally invariant state on the YC2n cylinder can be described by a uniform matrix product state (MPS) using $3n$ matrices, one for each site of the $1D$ unit cell. In contrast, the size of the YC2n - 2 unit cell is 6 independently of n . Since the numerical cost of the iDMRG algorithm varies linearly with the size of the unit cell, the YC2n - 2 geometry offers a significant

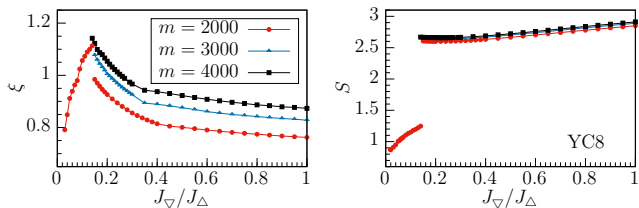


FIG. 2. Evolution of the correlation length ξ and entanglement entropy S of the ground state of the breathing kagome model Eq. (1) on an infinitely long YC8 cylinder. Up to $m = 4000$ states were kept in the S_z conserving DMRG simulation. For small J_∇/J_Δ , the results show negligible dependence on the bond dimension m .

computational advantage at large circumference n . We thus computed the ground state of Hamiltonian (1) in the YC8, YC8 – 2, YC10 – 2 and YC12 – 2 geometries.

In the isotropic limit $J_\nabla/J_\Delta = 1$, the ground state of the Hamiltonian Eq. (1) was identified as a time-reversal symmetric spin liquid in earlier works⁷. As noted in Refs. 7 and 18, DMRG simulations converge to a ground state with short range correlations on the cylinder geometry. We find that this behavior persists when a finite, and even relatively large amount of anisotropy is introduced in the model. Fig. 2 shows the evolution of various observables on the YC8 cylinder for several values of the anisotropy parameter J_∇/J_Δ , keeping up to $m = 4000$ states in the iDMRG simulation. The numerical results in the other cylinder geometries (YC8 – 2, YC10 – 2 and YC12 – 2) are given in the Appendix B. The correlation length is extracted from the two leading eigenvalues of the transfer matrix and thus conveniently obtained in our MPS formalism. The entanglement entropy is obtained for a bipartition of the system cutting the cylinder along the y axis. Both the correlation length and the entanglement entropy do not show any sign of a phase transition over a very wide interval of the anisotropy parameter ($J_\nabla/J_\Delta \geq 0.14$ in the YC8 geometry, and at least up to $J_\nabla/J_\Delta \simeq 0.2$ in all the considered cylinder geometries).

As can be seen in Fig. 2, all observables show a sharp transition at a value $J_\nabla/J_\Delta \simeq 0.14$. This transition also exists in the other geometries, albeit at different values of J_∇/J_Δ . We will discuss this phase transition in a later paragraph (see Sec. IV).

B. Low energy spectra from exact diagonalization

Additionally to our iDMRG analysis, we studied the model Eq. (1) using exact diagonalization. While only smaller system sizes can be reached with this technique, it is a method of choice to obtain the low-energy spectrum beyond the ground state. It also facilitates the exploration of systems preserving all spatial symmetries of the model.

We consider a finite kagome cluster with periodic

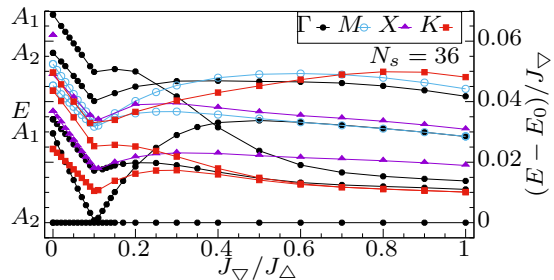


FIG. 3. Low energy spectrum of a kagome cluster with periodic boundary conditions and $N_s = 36$ spins. The states are labeled by their momentum sector and by the Mulliken symbol for the irreducible representation of D_3 in the Γ sector. The angular point at $J_\nabla/J_\Delta \simeq 0.10$ is due to a crossing between the ground states of the Γ_{A_1} and Γ_{A_2} sectors. A crossing occurs at an almost identical value of J_∇/J_Δ in the M sector. In the K sector, the breaking of inversion symmetry for $J_\nabla \neq J_\Delta$ results in the lifting of the associated degeneracy.

boundary conditions in both directions. We restrict ourselves to clusters with an even number of spins N_s to allow the formation of spin singlets in the system. As noted in Sec. II, the kagome lattice with breathing anisotropy has the symmetry of the dihedral group D_3 . The three smallest toroidal clusters which preserve this symmetry are made of $N_s = 12, 36$ and 48 spins. The $N_s = 48$ cluster is beyond our reach (its ground state across all sectors was recently obtained⁵¹ in the isotropic case – which preserves additional symmetries – at the cost of tremendous computational effort). This system can, however, be studied in the strongly anisotropic limit using the trimerized model Eq. (5) thanks to the dimensional reduction due to the projection onto local trimers. We will take advantage of this property in Sec. IV.

We obtained the low-energy spectrum for clusters up to $N_s = 36$ with several values of the breathing anisotropy (see Fig. 3 for $N_s = 36$ and Appendix A for the other sizes). The singlet-triplet gap remains large compared to the typical energy difference between successive energy levels, and we thus focus on the part of the spectrum with only singlets. The states are labeled by their momentum sector, as well as their eigenvalues under the D_3 operations when this symmetry is present. For all system sizes, the (normalized) low-energy spectrum is remarkably unaffected by an important change of the breathing anisotropy. Indeed, the relative positions of the first few eigenstates is unchanged for $0.55 \leq J_\nabla/J_\Delta \leq 1$ for all system sizes. More specifically, the smallest sizes ($N_s \leq 24$) do not show any gap closing above the ground state for any value of J_∇/J_Δ such that the ground states in the isotropic and strongly anisotropic limits are adiabatically connected. However in the $N_s = 30$ and 36 systems, the respective ground states in these two limits are characterized by different quantum numbers. The level crossing between the two states takes place respec-

tively at $J_{\nabla}/J_{\Delta} \simeq 0.4$ and $J_{\nabla}/J_{\Delta} \simeq 0.1$. The $N_s = 36$ system may be the most meaningful, since it preserves the full symmetry of the lattice. In this system, this transition corresponds to a crossing between the ground states of the Γ_{A_1} and Γ_{A_2} symmetry sectors (see Fig. 3).

The stability of the low-energy spectrum in all finite-size clusters confirms the robustness of the kagome spin liquid, in agreement with the iDMRG results of the previous paragraph. The largest clusters feature level crossings at very small values of J_{∇}/J_{Δ} . The similarity of these crossings with the one observed in the infinite cylinders – and the possibility that they might reveal the same phase transition – will be discussed in Sec. IV.

C. Signatures of Dirac cones using the transfer matrix spectrum

Using iDMRG, it is possible to obtain the momentum-resolved spectrum of correlation lengths, which is related to the excitation spectrum⁵². Ref. 20 has recently provided insights on the nature of the kagome ground state using this method at the isotropic point $J_{\nabla} = J_{\Delta}$. This study has reported signatures of Dirac cones, giving additional credibility to the hypothesis that the kagome ground state could be a Dirac spin liquid. The discrepancy between this observation and previous reports of a finite gap in DMRG studies was interpreted as a consequence of the wrapping of the system on a narrow cylinder. In this geometry, only few momentum values are allowed along the y direction. According to Ref. 20, the putative Dirac points fall on forbidden momenta leading to the opening of a finite gap to minimize the energy of the ground state.

We apply the same approach to the breathing kagome model. The momentum-resolved spectrum of correlation lengths is obtained from the leading eigenvalues of the transfer matrix, which is obtained from the MPS formulation of the ground state. Adiabatically inserting a flux θ along the cylinder axis is equivalent to twisting the boundary conditions of the cylinder, and reveals the properties of the system at various momenta. We use the YC8 – 2 geometry which provides a clear Dirac cone signature in Ref. 20. Our results are represented in Fig. 4 for $J_{\nabla}/J_{\Delta} = 1$ (reproducing the results of Ref. 20), 0.5, and 0.3. We show the inverted correlation length as a function of the twisting angle θ , and as function of the two momentum components (k_1, k_2) (defined in Fig. 1), which are extracted from the complex phase of the transfer matrix eigenvalues. The essential features stay the same throughout the phase. This includes similar Dirac cone signatures in the momentum-resolved spectrum.

We note that the data near the Dirac point $(2k_1, k_2) = (0, \pi)$ is missing in Fig. 4, which is because we cannot adiabatically insert flux when $\theta \sim \pi$. Physically it comes from the instability of the Dirac spin liquid on a quasi-1D system²⁰. One can in principle stabilize the Dirac spin liquid when $\theta \sim \pi$ by adding further neighbor interac-

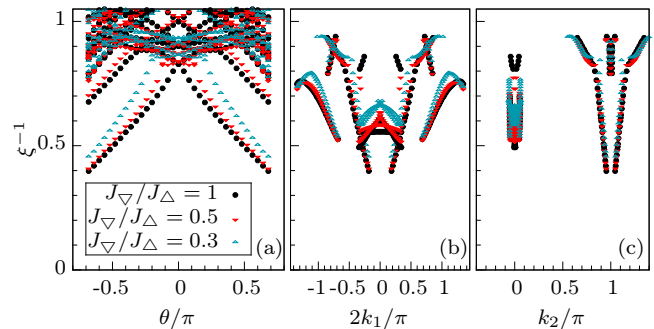


FIG. 4. (a) Evolution of the inverse of the correlation length ξ in the YC8 – 2 infinite cylinder upon adiabatic insertion of a flux θ for various values of the anisotropy parameter. $m = 4000$ states were kept in the DMRG simulation. (b, c) The momentum-resolved correlation length spectrum was extracted following the procedure outlined in Ref. 20.

tions (J_2) and by doing the adiabatic flux insertion with a smaller flux increment (see Ref. 20 for further details). We did not follow this direction here since the missing points do not obfuscate the main conclusion: both the Dirac cone structures and the instability of the spin liquid near $\theta \sim \pi$ persist from $J_{\nabla}/J_{\Delta} = 1$ to $J_{\nabla}/J_{\Delta} \sim 0.3$. This analysis – based on a probe very sensitive to any change of the ground state nature – confirms the remarkable robustness of the kagome spin liquid with regards to the breathing anisotropy.

We have explored the ground state properties of the kagome lattice model with breathing anisotropy. Several signatures – extracted from iDMRG and exact diagonalization – reveal a robust kagome spin liquid. The iDMRG study shows the existence of a phase transition at small J_{∇}/J_{Δ} , beyond which the ground state spontaneously breaks the discrete lattice rotational symmetry of the model. A transition is also observed in the largest finite clusters studied with exact diagonalization. In the following section, we focus on the strongly anisotropic regime of the model. We analyze the nature of the ground state in this regime and discuss the extrapolation of our results to the thermodynamic limit, in particular the existence of a phase transition at finite, but strong breathing anisotropy.

IV. PROBING THE STRONGLY ANISOTROPIC LIMIT

We now focus on the strongly anisotropic regime of Eq. (1) ($J_{\nabla}/J_{\Delta} < 0.2$). In most system geometries, we have observed a phase transition in this regime. In this section, we show that the ground state beyond the transition displays signatures of nematic order. We discuss the possible finite-size extrapolation of this result.

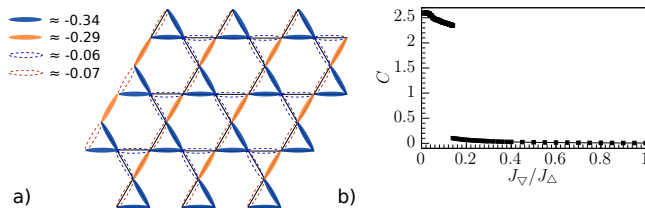


FIG. 5. (a) Neighboring spin-spin correlations in the ground state of the breathing kagome model in the limit $J_{\nabla}/J_{\Delta} \ll 1$. The numerical values were extracted from the ground state of H_{eff} on the YC12 geometry, obtained using iDMRG. (b) Evolution of the nematic order parameter C (9) of the ground state of the breathing kagome model Eq. (1) on an infinitely long YC8 cylinder. The results show negligible dependence on the bond dimension m , which was set to $m = 4000$ here.

A. Signatures of nematic order in the strongly anisotropic limit

We analyze the properties of the $J_{\nabla} < J_{\nabla}^c$ ground state using iDMRG and exact diagonalization. The main results are summarized here, and additional details can be found in Appendix B, C and D.

The iDMRG data reveals a spontaneous breaking of the rotational symmetry for $J_{\nabla} < J_{\nabla}^c$. The pattern of nearest-neighbor spin-spin correlations in the ground state is given in Fig. 5a. We can define a nematic order parameter C which measures the breaking of the three-fold rotational symmetry of the lattice:

$$C = \frac{2}{N_s} \sum_{\langle i,j \rangle} \gamma_{ij} \mathbf{S}_i \cdot \mathbf{S}_j \quad (9)$$

where the sum runs over all the nearest-neighbor spin pairs, and $\gamma_{ij} = e^{2\pi i \frac{l}{6}}$ is a phase defined by the direction of the $\langle i, j \rangle$ bond ($l = 0, 1, \dots, 5$ clockwise around each hexagon of the kagome lattice). The phase transition is easily detected by tracking the value of C as can be seen in Fig. 5b in the YC8 geometry (see Appendix B for the other cylinder geometries).

Note that the infinite cylinder geometry (which breaks the threefold rotational symmetry of the model) may influence the emergence of the nematic order. We thus turn to the exact diagonalization of finite clusters preserving all spatial symmetries of the model ($N_s = 12, 36, 48$). In this case, no spontaneous breaking of the D_3 symmetry can occur. Instead, we expect four low-lying states carrying the quantum numbers of the different representations of the dihedral group D_3 : E (doubly degenerate), A_1 and A_2 . The strong anisotropy spectra (obtained using the trimerized model of Sec. II B) are compatible with this prediction, even though they show a large finite-size splitting of the fourfold quasidegeneracy (see Appendix C). We also computed the spin-spin and dimer-dimer correlations of the ground state (see Appendix D). The former confirm the absence of spin-spin long-range order in the

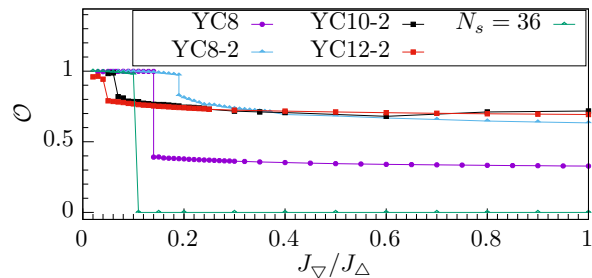


FIG. 6. Overlap of the ground state of the effective model Eq. (5) with the projected ground state of the breathing kagome model in the YC8, YC8 – 2, YC10 – 2 and YC12 – 2 geometries, and $N_s = 36$ spins toroidal cluster. On the infinite cylinder geometries, we show the overlap per site, extrapolated to $m \rightarrow \infty$ by using up to $m = 6000$ states in the iDMRG simulation.

anisotropic regime. The large dimer-dimer correlations form a pattern which mostly coincides with the pattern found with iDMRG. Finally, we studied the response of the ground state to a nematic perturbation. We found that the addition of an arbitrarily small D_3 -breaking term caused a significant response (finite value of C) in the strongly anisotropic regime and not for $J_{\nabla} > J_{\nabla}^c$ (see Appendix C). This confirms the large tendency to nematicity of the ground state of the kagome model with strong breathing anisotropy.

B. Connecting the ground states of the models with finite and infinite (trimerized) anisotropy

We used the effective model H_{eff} from Sec. II B to obtain the ground state in the strong anisotropy limit $J_{\nabla}/J_{\Delta} \ll 1$. It omits the high-energy degrees of freedom irrelevant in this limit, thus allowing to reach larger sizes: the toroidal clusters up to $N_s = 48$ for exact diagonalization, and up to YC12 cylinders with iDMRG. Consistently with the smaller sizes in the strongly anisotropic regime, we obtain a nematic ground state with short-range spin-spin correlations in the direction orthogonal to the stripes.

In the regime of small (but finite) J_{∇}/J_{Δ} , the high density of low-energy states in the exact kagome model (1) makes it difficult to converge to the ground state. This sets a lower bound to the accessible values of J_{∇}/J_{Δ} , leaving a blind area in the strong anisotropy regime. To learn about this regime, we have compared the ground states of (1) and H_{eff} . To compute their overlap, we must first project the kagome ground state $|\Psi_{J_{\nabla}/J_{\Delta}}\rangle$ onto the effective basis $\{\Delta\}$

$$\mathcal{P}_{\{\Delta\}} |\Psi_{\text{kag}}\rangle \quad (10)$$

This operation amounts to a projection of the local Hilbert space of each Δ triangle onto the $S = 1/2$ basis defined in Eq. (3). The overlap per site \mathcal{O} of the projected wave function with the ground state of H_{eff} is given for

all values of J_{∇}/J_{Δ} in Fig. 6. While \mathcal{O} is rather small (< 0.9) in the kagome spin liquid phase, it is very close to one ($\mathcal{O} > 0.99$) in the nematic phase. This very large overlap strongly suggests that the nematic ground state observed in the anisotropic kagome model for $J_{\nabla} < J_{\nabla}^c$ and the ground state of the effective model in fact correspond to the same phase. As a result, there would be at most two phases in the kagome model with breathing anisotropy, separated by a transition at $J_{\nabla} = J_{\nabla}^c$.

C. Finite-size extrapolation

The existence of a phase transition in the breathing kagome model (for a strong breathing anisotropy) is supported by numerical results from two different numerical techniques, iDMRG and exact diagonalization. From these results, we can draw a phase diagram involving the kagome spin liquid for $J_{\nabla}^c < J_{\nabla} \leq J_{\Delta}$, and a nematic state for $0 < J_{\nabla} < J_{\nabla}^c$. The existence of any other phases was ruled out in the accessible sizes by using a first order expansion of the trimerized model and relating its ground state to the ground state of the kagome model with $J_{\nabla} < J_{\nabla}^c$. Note that we have found a level crossing in all the geometries where the transition was observed. While this observation evokes a first-order phase transition, it is also compatible with a continuous transition in the case of a gapless spin liquid.

An important question is the significance of these results at the thermodynamic limit. With exact diagonalization, only few system sizes are available, and even fewer ($N_s = 12, 36$ and $N_s = 48$ in the trimerized limit) have the full symmetry of the lattice. The variety of behaviors concerning the existence and position of a phase transition in these systems is thus perhaps not so surprising. DMRG lets us explore cylinders with various perimeters and gives more consistent results, but the system's geometry might include an intrinsic bias towards the observed nematic state. Moreover, the value of the anisotropy at the transition shows a slight drift to smaller J_{∇}^c as the circumference is increased. This is especially clear when one considers the value of J_{∇}^c in the YC8 – 2, YC10 – 2 and YC12 – 2 geometries (respectively 0.19, 0.07, 0.05 as can be seen in Fig. 6). Since only a few cylinder perimeters are available, it is difficult to extrapolate the value of J_{∇}^c to the thermodynamic limit. We cannot completely rule out the possibility that it might become zero in the thermodynamic limit, and that the nematic ground state might be unstable at finite J_{∇} .

V. CONCLUSION

We have numerically studied the influence of the breathing anisotropy on the ground state of the kagome nearest-neighbor antiferromagnet. Using a variety of methods based on DMRG and exact diagonalization, we have shown that the kagome spin liquid antiferromagnet

is extremely stable to the breathing anisotropy. The variety of system geometries (infinitely long cylinder and torus) and sizes is a strong argument to argue that this finding may remain qualitatively true in the thermodynamic limit and should apply to the kagome material DQVOF. Indeed, even our most conservative estimation of the stability regime ($J_{\nabla}/J_{\Delta} > 0.2$) includes the value measured in this material ($J_{\nabla}/J_{\Delta} \simeq 0.55$ according to a very recent estimation²⁷). DQVOF thus appears as an excellent candidate to realize the kagome spin liquid. Moreover, we have found signatures of Dirac cones in the ground state of the breathing kagome model which are compatible with the experimental observation of a gapless spin liquid in DQVOF. These signatures are essentially the same as the ones already observed in the isotropic model²⁰.

Beyond the connection to existing materials, we have discussed the existence of a phase transition at $J_{\nabla}/J_{\Delta} < 0.2$. Such transition appears for all the cylinder geometries that we studied, as well as in the largest toroidal cluster that we were able to diagonalize (36 spins). Considering the large dependency of the breathing anisotropy at the transition J_{∇}^c with system size (from 0.05 for the YC12 – 2 cylinder to 0.2 for the YC8 – 2 cylinder), it is hard to extrapolate these findings to the thermodynamic limit. In fact, the transition value seems to decrease when the cylinder perimeter increases in the YC2n – 2 geometry. Whether or not this value remains finite at the thermodynamic limit remains to be determined.

We have also investigated the nature of the ground state in the strongly anisotropic (trimerized) limit. On the cylinder geometry, for the accessible perimeters, the ground state has nematic order. On the torus geometry (considering only geometries which preserve the rotational symmetry of the model), the analysis of the ground state has shown a large tendency to nematicity. The quantum numbers of the lowest energy states in the 36 and 48 spins cluster are in agreement with this hypothesis, but the spectra show large finite size effects. Using an effective trimerized model has allowed us to explore numerically the very anisotropic regime of the phase diagram. Interestingly, the phase diagram seems to consist of at most two phases: one connected to the ground state of the trimerized model, and one connected to the kagome spin liquid.

The nematic phase in the strongly anisotropic (trimerized) limit preserves the translational symmetry, the spin rotation symmetry and it has spin-3/2 per unit cell. Therefore according to the Hastings-Oshikawa-Lieb-Schultz-Mattis theorem⁵³⁻⁵⁶, one cannot adiabatically deform this nematic phase into a trivial product state. This leads to interesting possibilities, for example the nematic phase could be a 2D (nematic) spin liquid. The other possibility is that the nematic phase is made of decoupled 1D Luttinger liquids even though the original trimerized model is 2D isotropic. Understanding the nematic phase and the phase transition might lead to new insight on the kagome spin liquid.

VI. ACKNOWLEDGMENTS

We thank D. Poilblanc, A. Tsirlin, N. Regnault and M. Mambrini for insightful discussions, and especially Roderich Moessner for collaboration during the early stages of this work. This work was supported in parts

by the German Research Foundation (DFG) via SFB 1143 and Research Unit FOR 1807. YCH is supported by a postdoctoral fellowship from the Gordon and Betty Moore Foundation, under the EPIQS initiative, GBMF4306, at Harvard University.

-
- ¹ P. Anderson, *Materials Research Bulletin* **8**, 153 (1973).
² X. G. Wen, *International Journal of Modern Physics B* **04**, 239 (1990).
³ L. Savary and L. Balents, *ArXiv e-prints* (2016), arXiv:1601.03742 [cond-mat.str-el].
⁴ P. W. Anderson, *Science* **235**, 1196 (1987).
⁵ P. A. Lee, *Science* **321**, 1306 (2008).
⁶ L. Balents, *Nature* **464**, 199 (2010).
⁷ S. Yan, D. A. Huse, and S. R. White, *Science* **332**, 1173 (2011).
⁸ N. Read and S. Sachdev, *Phys. Rev. Lett.* **66**, 1773 (1991).
⁹ K. Yang, L. K. Warman, and S. M. Girvin, *Phys. Rev. Lett.* **70**, 2641 (1993).
¹⁰ M. B. Hastings, *Phys. Rev. B* **63**, 014413 (2000).
¹¹ V. Elser, *Phys. Rev. Lett.* **62**, 2405 (1989).
¹² J. B. Marston and C. Zeng, *Journal of Applied Physics* **69**, 5962 (1991).
¹³ P. Nikolic and T. Senthil, *Phys. Rev. B* **68**, 214415 (2003).
¹⁴ R. R. P. Singh and D. A. Huse, *Phys. Rev. B* **76**, 180407 (2007).
¹⁵ G. Ewenbly and G. Vidal, *Phys. Rev. Lett.* **104**, 187203 (2010).
¹⁶ Y. Ran, M. Hermele, P. A. Lee, and X.-G. Wen, *Phys. Rev. Lett.* **98**, 117205 (2007).
¹⁷ Y. Iqbal, F. Becca, S. Sorella, and D. Poilblanc, *Phys. Rev. B* **87**, 060405 (2013).
¹⁸ S. Depenbrock, I. P. McCulloch, and U. Schollwöck, *Phys. Rev. Lett.* **109**, 067201 (2012).
¹⁹ H.-C. Jiang, Z. Wang, and L. Balents, *Nature Physics* **8**, 902 (2012), arXiv:1205.4289 [cond-mat.str-el].
²⁰ Y.-C. He, M. P. Zaletel, M. Oshikawa, and F. Pollmann, *ArXiv e-prints* (2016), arXiv:1611.06238 [cond-mat.str-el].
²¹ J. S. Helton, K. Matan, M. P. Shores, E. A. Nytko, B. M. Bartlett, Y. Yoshida, Y. Takano, A. Suslov, Y. Qiu, J.-H. Chung, D. G. Nocera, and Y. S. Lee, *Phys. Rev. Lett.* **98**, 107204 (2007).
²² H. Yoshida, Y. Okamoto, T. Tayama, T. Sakakibara, M. Tokunaga, A. Matsuo, Y. Narumi, K. Kindo, M. Yoshida, M. Takigawa, and Z. Hiroi, *Journal of the Physical Society of Japan* **78**, 043704 (2009).
²³ Z. Hiroi, M. Hanawa, N. Kobayashi, M. Nohara, H. Takagi, Y. Kato, and M. Takigawa, *Journal of the Physical Society of Japan* **70**, 3377 (2001).
²⁴ Y. Okamoto, H. Yoshida, and Z. Hiroi, *Journal of the Physical Society of Japan* **78**, 033701 (2009).
²⁵ F. H. Aidoudi, D. W. Aldous, R. J. Goff, S. M. Z., J. P. Attfield, R. E. Morris, and P. Lightfoot, *Nature Chemistry* **3**, 801 (2011).
²⁶ L. Clark, J. C. Orain, F. Bert, M. A. De Vries, F. H. Aidoudi, R. E. Morris, P. Lightfoot, J. S. Lord, M. T. F. Telling, P. Bonville, J. P. Attfield, P. Mendels, and A. Harrison, *Phys. Rev. Lett.* **110**, 207208 (2013).
²⁷ J.-C. Orain, B. Bernu, P. Mendels, L. Clark, F. H. Aidoudi, P. Lightfoot, R. E. Morris, and F. Bert, *Phys. Rev. Lett.* **118**, 237203 (2017).
²⁸ Y.-C. He, D. N. Sheng, and Y. Chen, *Phys. Rev. Lett.* **112**, 137202 (2014).
²⁹ S.-S. Gong, W. Zhu, and D. N. Sheng, *Scientific Reports* **4**.
³⁰ Y.-C. He and Y. Chen, *Phys. Rev. Lett.* **114**, 037201 (2015).
³¹ A. M. Läuchli and R. Moessner, *ArXiv e-prints* (2015), arXiv:1504.04380 [cond-mat.quant-gas].
³² H. J. Changlani, D. Kochkov, K. Kumar, B. K. Clark, and E. Fradkin, *ArXiv e-prints* (2017), arXiv:1703.04659 [cond-mat.str-el].
³³ Y.-C. He, Y. Fuji, and S. Bhattacharjee, *ArXiv e-prints* (2015), arXiv:1512.05381 [cond-mat.str-el].
³⁴ F. Mila, *Phys. Rev. Lett.* **81**, 2356 (1998).
³⁵ M. E. Zhitomirsky, *Phys. Rev. B* **71**, 214413 (2005).
³⁶ V. Subrahmanyam, *Phys. Rev. B* **52**, 1133 (1995).
³⁷ C. Raghun, I. Rudra, S. Ramasesha, and D. Sen, *Phys. Rev. B* **62**, 9484 (2000).
³⁸ R. Budnik and A. Auerbach, *Phys. Rev. Lett.* **93**, 187205 (2004).
³⁹ S. Capponi, A. Läuchli, and M. Mambrini, *Phys. Rev. B* **70**, 104424 (2004).
⁴⁰ R. Schaffer, Y. Huh, K. Hwang, and Y. B. Kim, *Phys. Rev. B* **95**, 054410 (2017).
⁴¹ M. Mambrini and F. Mila, *The European Physical Journal B - Condensed Matter and Complex Systems* **17**, 651 (2000).
⁴² K. I. Kugel and D. I. Khomskii, *Phys. Usp.* **25**, 231 (1982).
⁴³ K. Penc, M. Mambrini, P. Fazekas, and F. Mila, *Physical Review B* **68**, 012408 (2003).
⁴⁴ Y. Q. Li, M. Ma, D. N. Shi, and F. C. Zhang, *Phys. Rev. Lett.* **81**, 3527 (1998).
⁴⁵ F. Vernay, K. Penc, P. Fazekas, and F. Mila, *Phys. Rev. B* **70**, 014428 (2004).
⁴⁶ S. R. White, *Phys. Rev. Lett.* **69**, 2863 (1992).
⁴⁷ U. Schollwöck, *Rev. Mod. Phys.* **77**, 259 (2005).
⁴⁸ U. Schollwöck, *Annals of Physics* **326**, 96 (2011), arXiv:1008.3477 [cond-mat.str-el].
⁴⁹ E. M. Stoudenmire and S. R. White, *Annual Review of Condensed Matter Physics* **3**, 111 (2012).
⁵⁰ J. A. Kjäll, M. P. Zaletel, R. S. K. Mong, J. H. Bardarson, and F. Pollmann, *Phys. Rev. B* **87**, 235106 (2013).
⁵¹ A. M. Läuchli, J. Sudan, and R. Moessner, *ArXiv e-prints* (2016), arXiv:1611.06990 [cond-mat.str-el].
⁵² V. Zauner, D. Draxler, L. Vanderstraeten, M. Degroote, J. Haegeman, M. M. Rams, V. Stojevic, N. Schuch, and F. Verstraete, *New Journal of Physics* **17**, 053002 (2015).
⁵³ E. Lieb, T. Schultz, and D. Mattis, *Annals of Physics* **16**, 407 (1961).
⁵⁴ M. Oshikawa, *Phys. Rev. Lett.* **84**, 1535 (2000).

⁵⁵ G. Misguich, C. Lhuillier, M. Mambrini, and P. Sindzingre, The European Physical Journal B - Condensed Matter and Complex Systems **26**, 167 (2002).

⁵⁶ M. B. Hastings, EPL (Europhysics Letters) **70**, 824 (2005).

Appendix A: Stability of the kagome spin liquid: exact diagonalization of small clusters

In the main text, we have given the result of the exact diagonalization of the largest toroidal clusters preserving the full D_3 symmetry of the Hamiltonian – i.e. 36 spins, and 48 spins in the very anisotropic limit. In Fig. 7, we give the results obtained for the other clusters: $N_s = 12$ (which preserves D_3) and $N_s = 18, 24, 30$ (which break D_3). There are significant finite-size effects, but all geometries show a large robustness of the kagome ground state with breathing anisotropy. $N_s = 30$ is the smallest size for which we observe a closing of the singlet-singlet gap.

Appendix B: iDMRG results on the YC2n – 2 cylinder geometries

In this section, we give the result of our iDMRG calculations on the geometries YC8 – 2 (Fig. 8), YC10 – 2 (Fig. 9) and YC12 – 2 (Fig. 10). They complete the results obtained on the YC8 geometry in Fig. 2, and confirm the conclusions of Sec. III regarding the very large stability of the kagome spin liquid with breathing anisotropy. We also track the phase transition to a nematically ordered state.

To evaluate the influence of truncation, we did a scaling of the bond dimension m . In the YC12 – 2 cylinder where the influence of truncation is the largest, we note a shift of the phase transition towards smaller values of J_∇^c as m becomes larger. The effect of the finite bond dimension is thus to underestimate the stability of the kagome spin liquid. This phenomenon has a simple explanation: the nematic ground state ($J_\nabla < J_\nabla^c$) has a much smaller entanglement entropy than its symmetry-preserving ($J_\nabla > J_\nabla^c$) counterpart, and can be much more efficiently represented in the MPS language. Indeed, the bonds with strong correlations are almost always nearest neighbors in the one-dimensional snake used to map the 2D lattice to a 1D chain. We verified that a different choice for the DMRG snake did not have a significant influence on our results, and especially on the value of J_∇^c . In practice, we explored the values $J_\nabla > J_\Delta$. In the limit of infinite bond dimensions, this is equivalent to $J_\nabla < J_\Delta$, but it can lead to different results for small bond dimensions since it corresponds to a different 1D-to-2D mapping. For the YC8 geometry, we found the value of the transition to be within a 5% error margin of the value obtained for $J_\nabla < J_\Delta$ after bond dimension extrapolation.

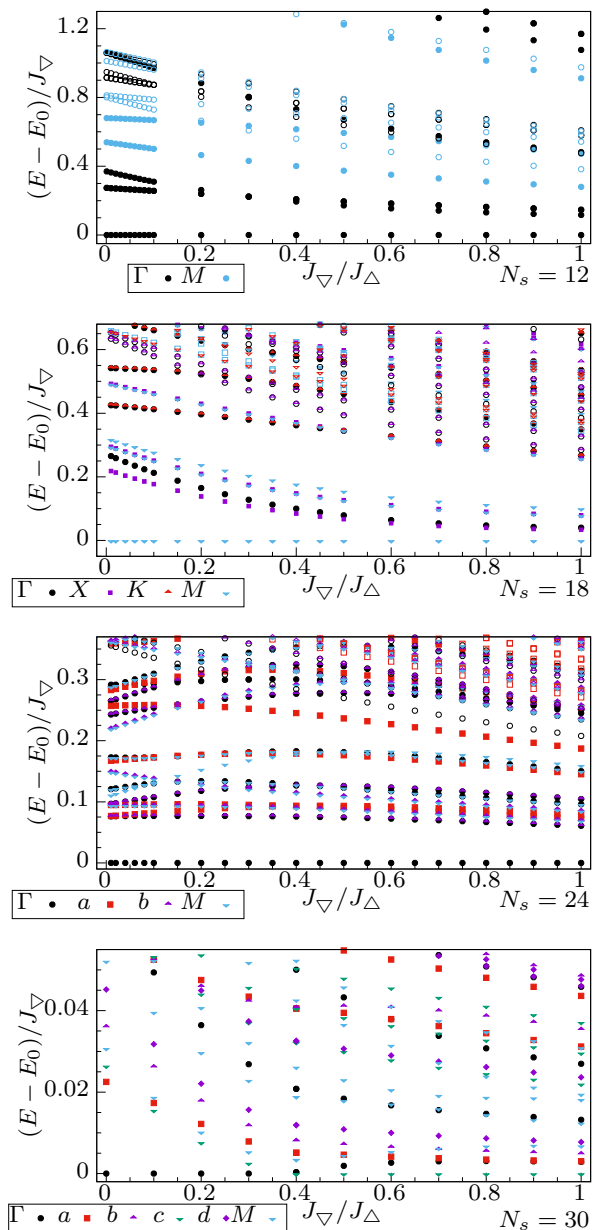


FIG. 7. Low energy spectrum of several kagome lattice clusters with N_s spins and periodic boundary conditions. The filled (respectively empty) symbols correspond to even (respectively odd) values of S . The different colors correspond to different momentum sectors.

Appendix C: Additional evidence of nematic order in the strongly anisotropic regime: exact diagonalization of toroidal clusters

1. Quasidegeneracy

As stated in the main text, in finite size systems, the spontaneous breaking of the D_3 symmetry should result in a fourfold quasidegeneracy of the ground state (an A_1

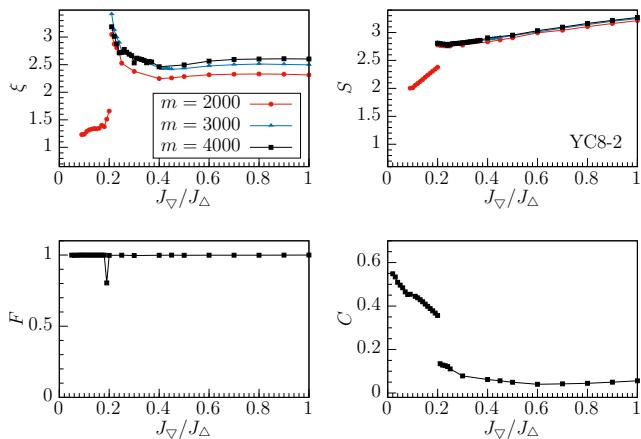


FIG. 8. Evolution of the correlation length ξ , entanglement entropy S , and fidelity per ring F and nematic order parameter C Eq. (9) of the ground state of the breathing kagome model Eq. (1) on an infinitely long YC8 – 2 cylinder. Up to $m = 4000$ states were kept in the DMRG simulation.

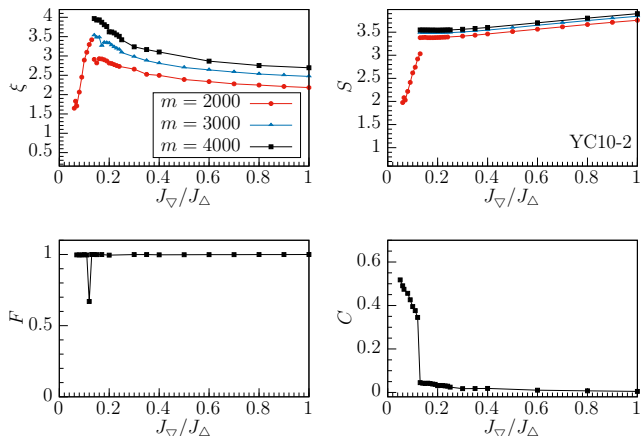


FIG. 9. Evolution of the correlation length ξ , entanglement entropy S , and fidelity per ring F and nematic order parameter C Eq. (9) of the ground state of the breathing kagome model Eq. (1) on an infinitely long YC10 – 2 cylinder. Up to $m = 4000$ states were kept in the DMRG simulation.

state, an A_2 state, and two exactly degenerate E states). Focusing on the spectrum of the D_3 -preserving clusters $N_s = 12, 36, 48$, we note that the three lowest energies in the Γ sector correspond indeed respectively to A_1 , A_2 and E . These are also the three lowest energies of the system irrespective of momentum sector for $N_s = 48$ (see Fig. 11). This is also the case for $N_s = 12$, although this is perhaps less meaningful given the very small system size. In the three geometries, the finite-size effects are strong, and there is a large splitting between the four low-lying states.

We focus on the $N_s = 48$ system. We cannot obtain the full phase diagram (the isotropic point – which has additional symmetries – was recently obtained in Ref. 51 at

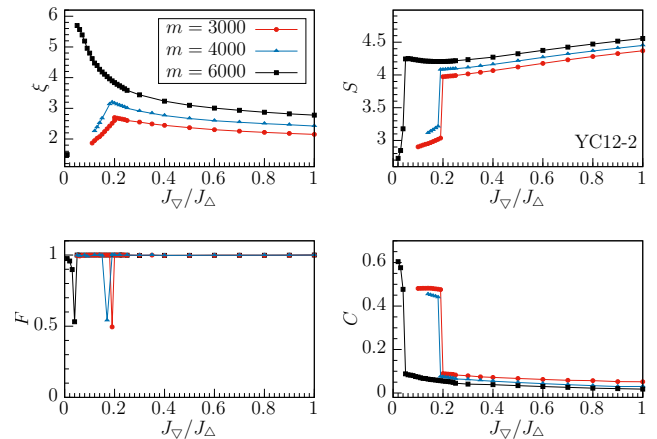


FIG. 10. Evolution of the correlation length ξ , entanglement entropy S , and fidelity per ring F and nematic order parameter C Eq. (9) of the ground state of the breathing kagome model Eq. (1) on an infinitely long YC12 – 2 cylinder. Up to $m = 6000$ states were kept in the DMRG simulation.

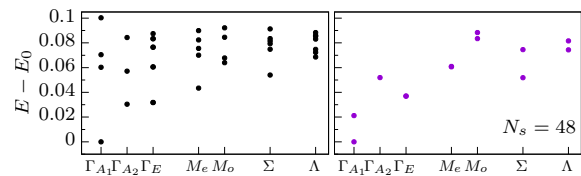


FIG. 11. Low energy spectrum of a kagome cluster with periodic boundary conditions and $N_s = 48$ spins. The states are labeled by their momentum sector and by the Mulliken symbol for the irreducible representation of D_3 in the Γ sector, as well as parity under reflection in the M sector. We show the low-energy spectrum of the trimerized model H_{eff} (left), and, for reference, the low-energy spectrum of the isotropic model (right) as given in Ref. 51.

colossal computational cost). However, we can compare the spectra in the strongly anisotropic limit (obtained by exact diagonalization of H_{eff}) and at the isotropic point (given in Ref. 51). The two corresponding low-energy spectra are given in Fig. 11. The absolute ground states in either limit fall in the same sector (Γ_{A_1}), but the first few excitations (which are in the Γ sector) have different quantum numbers. The reorganization of the low energy states within the Γ sector is compatible with a phase transition to a nematic phase. While this interpretation cannot be categorically favored, it seems consistent with our observations in other system geometries.

2. Response to a nematic perturbation

The emergence of a nematic ground state may be hard to detect, since finite-size effects can lift the expected quasidegeneracy to a large extent. Studying the response

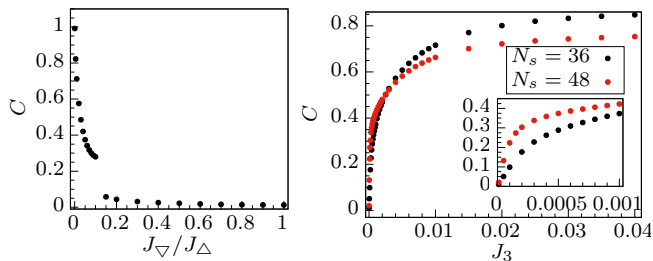


FIG. 12. Response of the ground state of a finite toroidal cluster (obtained using ED) to a D_3 -breaking perturbation H_3 (see Eq. (C1)). The nematic order parameter C is defined in Eq. (9). a) The response to the nematic perturbation is measured for various values of J_∇/J_Δ in the $N_s = 36$ system (using the full model Eq. (1)), while the perturbation is fixed to $J_3 = 0.001$. b) H_3 is adiabatically added to a system with N_s spins and $J_\nabla/J_\Delta = 0.01$. The ground state of the system was obtained using the effective model eq. (5). A zoom-in plot is presented in the inset.

of the ground state to a small D_3 -breaking perturbation term can help us quantify the system's proneness to nematicity. We consider the following perturbation

$$H_3 = J_3 \left(J_\Delta \sum_{\langle i,j \rangle \in \Delta'} \mathbf{S}_i \cdot \mathbf{S}_j + J_\nabla \sum_{\langle i,j \rangle \in \nabla'} \mathbf{S}_i \cdot \mathbf{S}_j \right) \quad (\text{C1})$$

where Δ' (respectively ∇') defines the dimers of the upward (resp. downward) triangle with the largest correlation (full blue and orange bonds in Fig. 5). H_3 explicitly breaks D_3 and favors the formation of a nematic state with a short-range correlation pattern similar to the one observed in the DMRG study of YC2n cylinders (Fig. 5).

We present the response of the ground state of the $N_s = 36$ and $N_s = 48$ toroidal clusters to the addition of H_3 in Fig. 12. We start by evaluating the nematic response (9) across the whole phase diagram. This can be done after diagonalization of the interaction $H + H_3$ in the full Hilbert space for a system of $N_s = 36$ spins. For a small symmetry-breaking term $J_3 = 0.001$, the nematic response is very small at the isotropic point ($C = 0.01$), and remains of the same order of magnitude for $J_\nabla/J_\Delta > 0.1$ ($C < 0.06$) as can be seen in Fig. 12a. At $J_\nabla/J_\Delta > 0.1$, we observe a phase transition, with a jump to $C = 0.28$, and an increasingly large response in the strongly anisotropic regime. Note that the position of the jump corresponds to the level crossing in the ground state of the original ($J_3 = 0$) model studied in Sec. III B. This is in agreement with the much stronger tendency to nematicity in the strongly anisotropic regime already

observed on infinite cylinders.

Focusing on the strongly anisotropic regime, we added H_3 adiabatically to the original Hamiltonian at $J_\nabla/J_\Delta = 0.01$, using the effective trimerized model for the diagonalization (see Fig. 12b). Using this model allows us to access the next system with D_3 symmetry ($N_s = 48$). For both accessible system sizes, there is a finite response even for arbitrarily small perturbations, and a sharp increase of C with increasing J_3 (even sharper for the largest system size). This confirms the instability of the ground state to a (seemingly arbitrarily small) nematic perturbation.

Appendix D: Correlations of the ground state of the kagome model with strong breathing anisotropy on toroidal clusters

In this section, we give the correlation functions of the ground state in the strong breathing anisotropy regime. From the ground state of the effective trimerized model Eq. (5), we extracted the spin-spin correlation function

$$S(i) = \langle \mathbf{S}_0 \cdot \mathbf{S}_i \rangle \quad (\text{D1})$$

and the connected spin-spin correlation function

$$S_c(i) = \langle \mathbf{S}_0 \cdot \mathbf{S}_i \rangle - \langle \mathbf{S}_0 \rangle \langle \mathbf{S}_i \rangle \quad (\text{D2})$$

where 0 is the index used to label the reference spin. Similarly, we also extracted the dimer-dimer correlation function and its connected counterpart

$$\begin{aligned} D(\langle i, j \rangle) &= \langle \mathbf{S}_0 \cdot \mathbf{S}_1 \mathbf{S}_i \cdot \mathbf{S}_j \rangle \\ D_c(\langle i, j \rangle) &= \langle \mathbf{S}_0 \cdot \mathbf{S}_1 \mathbf{S}_i \cdot \mathbf{S}_j \rangle - \langle \mathbf{S}_0 \cdot \mathbf{S}_1 \rangle \langle \mathbf{S}_i \cdot \mathbf{S}_j \rangle \end{aligned} \quad (\text{D3})$$

where $\langle i, j \rangle$ corresponds to two neighboring spins. The correlation functions are extracted from the ground state obtained by exact diagonalization of the $N_s = 36, 48$ systems (Figs. 13 for the spin-spin correlations, 14 for the dimer-dimer correlations) or iDMRG in the YC8 geometry (Fig. 15 for the dimer-dimer correlations). In the latter case, the ground state spontaneously breaks the D_3 symmetry, and we thus do not use the connected correlation function, which is close to zero at all points. We also give the correlations in the $N_s = 36$ ground state of the isotropic Heisenberg model for reference.

The rapid decay of the spin-spin correlations confirms the disordered nature of the ground state. The dimer-dimer correlations, however, remain finite at relatively large distances in the strong breathing anisotropy regime. Similar patterns can be identified on the torus and infinite cylinder geometries, such as stronger correlations between dimers of the same orientation.

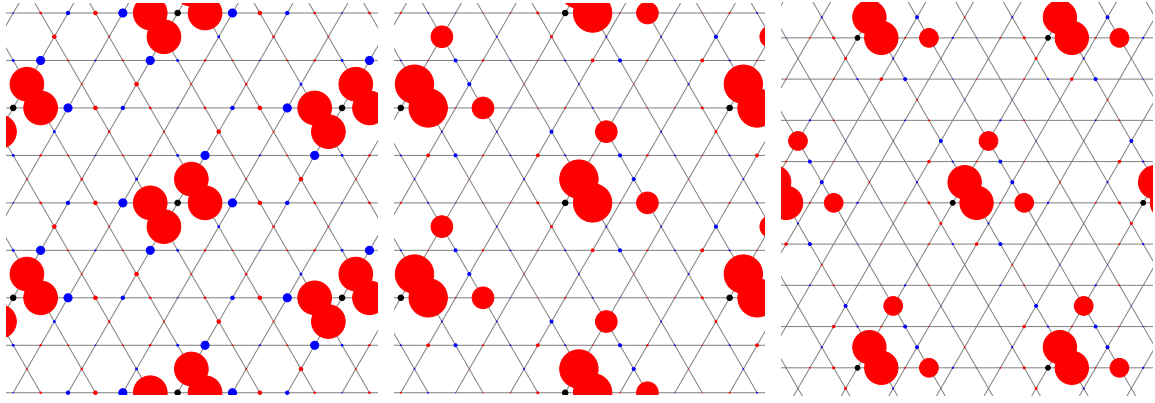


FIG. 13. Connected spin-spin correlation function S_c of the ground state of the heisenberg model (left) with $N_s = 36$ spins, the trimerized kagome model with 36 (middle) and 48 (right) spins. The reference site is indicated in black.

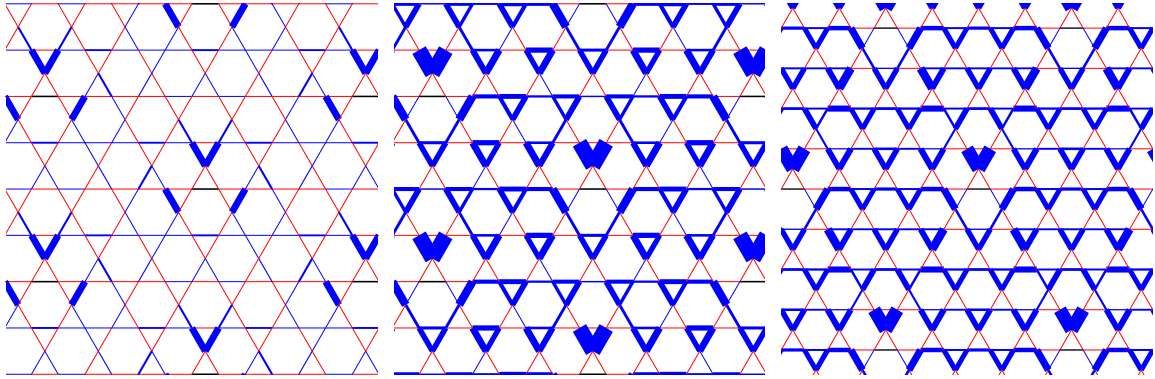


FIG. 14. Connected dimer-dimer correlation function D_c the ground state of the heisenberg model (left) with $N_s = 36$ spins, the trimerized kagome model with 36 (middle) and 48 (right) spins. The reference dimer is indicated in black

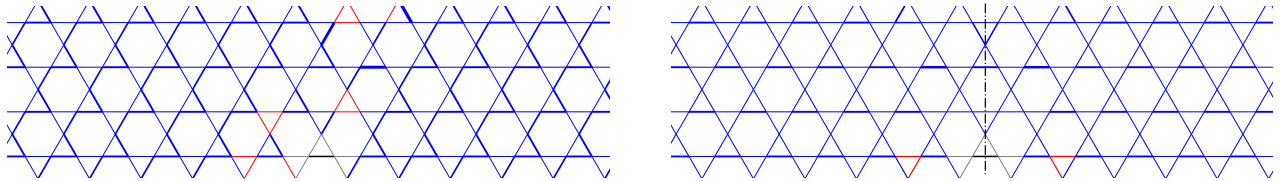


FIG. 15. Dimer-dimer correlation function D of the ground state of the trimerized kagome model on the YC8 cylinder. The reference dimer is indicated in black. On the right panel, we have symmetrized the correlation function with respect to the black dashed line to facilitate the comparison with the ED results (Fig. 14), where this reflection is an exact symmetry.